Ultrasonics Sonochemistry 94 (2023) 106330

Contents lists available at ScienceDirect

Ultrasonics Sonochemistry

journal homepage: www.elsevier.com/locate/ultson

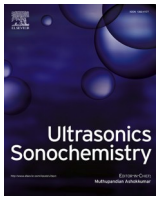

Ultrasound-pretreatment combined with Ti_3C_2-TiO_2-AuNPs enhancing the electrogenerated chemiluminescence of the air-saturated luminol for exosomes detection

Huixin Zhang, Xin Zhou, Feifei Zhang, Jianfei Xia, Zonghua Wang *

College of Chemistry and Chemical Engineering, College of Materials Science and Engineering, Shandong Sino-Japanese Centre for Collaborative Research of Carbon Nanomaterials, Instrumental Analysis Centre of Qingdao University, Qingdao University, Qingdao, Shandong 266071, China

ARTICLE INFO

Keywords:
Ultrasound-pretreatment
Ti_3C_2-TiO_2-AuNPs
Electrogenerated chemiluminescence
The air-saturated luminol
ROS

ABSTRACT

It is still a great challenge to develop effective strategies to improve the low electrogenerated chemiluminescence (ECL) of air-saturated luminol. Herein, the synergistic effects of Ti_3C_2-TiO_2-AuNPs nano hybrid and high-intensity focused ultrasound pretreatment (ultrasound-pretreatment) were used to significantly improve the ECL emission of the air-saturated luminol, and the mechanism was proposed. The ultrasound-pretreatment as a green method with the cavitation effect could form $O_2^{\bullet-}$ and H_2O_2 in situ as an initiator. TiO_2 and Au nanoparticles (AuNPs) were in situ decorated on the Ti_3C_2 surface to form Ti_3C_2-TiO_2-AuNPs, and it was proved as a highly efficient booster which could catalyze and aggregate H_2O_2 to the $O_2^{\bullet-}$. The utilization rate of intermediates has been greatly improved. Exosomes as model targets can be sensitively detected by the ECL sensor. The detection limit was 195 particles μL^{-1}. The detection results of exosomes in actual samples are satisfactory. We believe that the ultrasound-pretreatment strategy could be extended to the sensitive detection in the biological sample.

1. Introduction

Luminol is a classic organic ECL emitter, which is favored because of its low oxidation potential, nontoxicity, and so on [1–3]. In the air-saturated luminol, dissolved oxygen with low toxicity and natural stability is a potential and green endogenous coreactant of luminol [4–6]. However, the low content and conversion rate of dissolved oxygen result unsatisfied ECL intensity of luminol. To solve the problem, coreactants are usually introduced to activate the air-saturated luminol to generate more the reactive oxygen species (ROS). So far, numerous species, such as, enzymes, nanomaterials (Cu_2O@AuNPs, Pt-Au@ZnO and Au-Ag-Pt heteronanostructures [7–9] and single-atom catalysts [10–13]) have been developed as the accelerator to promote conversion of O_2 to ROS. The developing of green and effective means to boost the ECL strength of the air-saturated luminol is still a hot topic.

It should be noted that ultrasound, as a unique non-invasive means, has played a significant role in biochemical research and clinical treatment [14,15]. Among them, high-intensity focused ultrasound has the inherent advantages of reducing off target damage and improving ultrasound dept, which is considered to be one of the most promising minimally invasive methods [16,17]. High negative pressure in the ultrasound focus area can generate cavitation bubbles, then the cavitation bubbles oscillate and collapse. In the process of bubble shrinkage, the internal gas is compressed, resulting in the decomposition of water molecules and O_2 to generate ROS, such as $O_2^{\bullet-}$, $^1O_2$, H_2O_2 and so on [18,19]. So far, only a few papers on the application of ultrasound in ECL have been reported [20,21]. Our research group has done the related work in the field of ECL sensing, especially in improving selectivity and sensitivity by using nanomaterials [3,5]. We speculated that the combination of ultrasound and nanomaterials will be a potential means to boost ECL signal of air-saturated luminol.

Titanium dioxide (TiO_2) has become an emerging material in recent years in the biosensing [22–25]. It was reported that TiO_2 could catalyze the oxidation of H_2O_2 and aggregate ROS, such as $O_2^{\bullet-}$ and •OH owing to the band gap dependent catalytic performance of TiO_2, which contributes significantly to the ECL emission of luminol [26]. Recently, based on TiO_2 nano-hybrid, such as AuAg/TiO_2 [27], Att-TiO_2 [28], Fe_3O_4-TiO_2@NH_2 [29] with strong catalytic performance and good conductivity have attracted much attention in the ECL sensing. However, pre-synthesis of TiO_2 usually requires multi-step process and the

* Corresponding author.
E-mail address: wangzonghua@qdu.edu.cn (Z. Wang).

https://doi.org/10.1016/j.ultsonch.2023.106330
Received 20 December 2022; Received in revised form 30 January 2023; Accepted 11 February 2023
Available online 13 February 2023

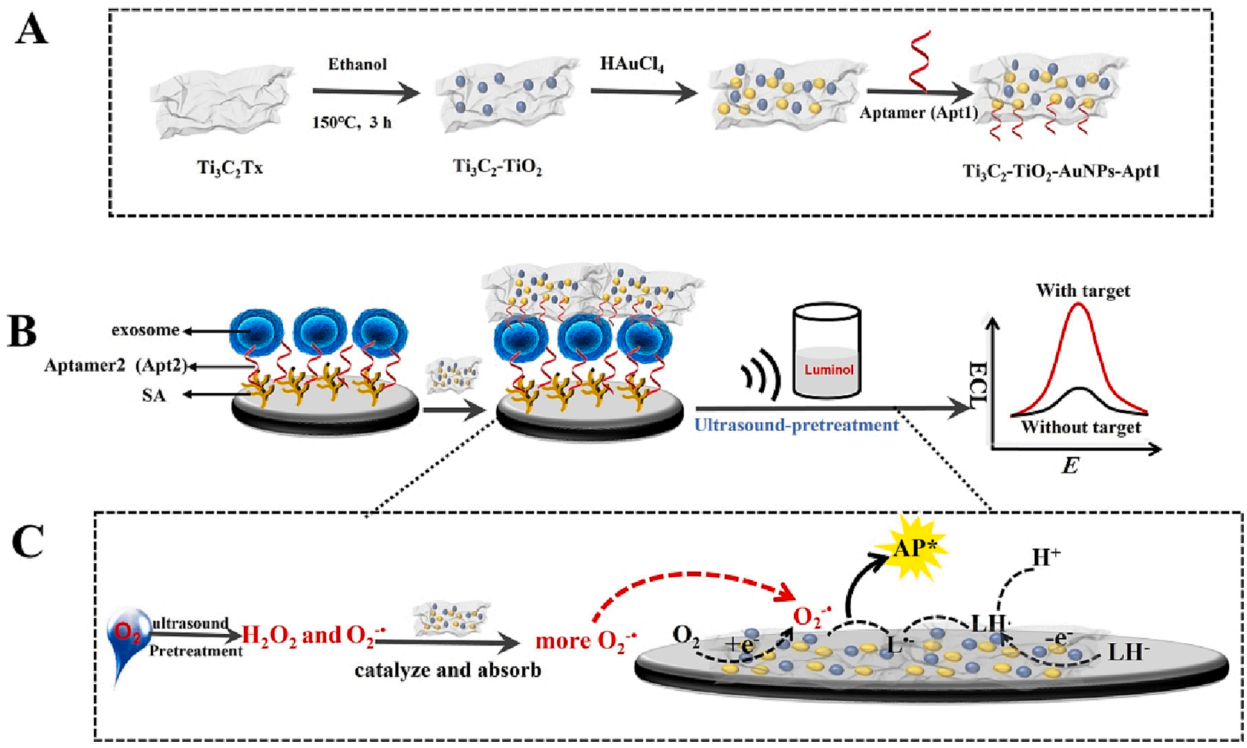

Scheme 1. (A) Synthesis of Ti_3C_2-TiO_2-AuNPs nanoprobes. (B) ECL platform for target detection. (C) The illustration of the synergistic effect of ultrasound-pretreatment and Ti_3C_2-TiO_2-AuNPs for the air-saturated luminol.

synthesized TiO_2 has a large size, leading to small specific surface area and relatively few active sites of the nano-hybrid. Therefore, it is necessary to find an effective and easy synthesis method of TiO_2 with small size to exert its excellent performance in the ECL biosensing. In situ growth of TiO_2 on the nanomaterial could be a promising approach. Fortunately, Ti_3C_2 MXenes as a novel two-dimensional nanomaterial has rich exposed metal sites, excellent reducibility, catalysis and electrical conductivity [30–36], which can provide rich Ti source to generate the small size of TiO_2 in situ. Ti_3C_2 nanosheets can be used as support platform for TiO_2, which can effectively prevent the self-aggregation of TiO_2. We expected the Ti_3C_2-TiO_2 generated in situ has an effect of "two birds with one stone" to enhance the ECL response of the air-saturated luminol.

In the present work, we designed a ECL platform with synergistic effect to achieve the goal of sensitive determination of exosomes (Scheme 1). Ultrasound with ultrasonic cavitation effect was a pre-treatment means and TiO_2 and AuNPs were generated in situ on Ti_3C_2 to form Ti_3C_2-TiO_2-AuNPs as nanoprobes. The Ti_3C_2-TiO_2-AuNPs nanoprobes can catalyze H_2O_2 and aggregate ROS generated from ultrasound-pretreatment via cavitation ingeniously to greatly boost the ECL emission of the air-saturated luminol. In the Scheme 1A, the Ti_3C_2-TiO_2-AuNPs nano hybrid was formed by the reducibility of Ti. The Scheme 1B shows the construction of ECL sensor for exosome detection. The CD63 aptamer2 (Apt2) was modified on sodium alginate (SA). Moreover, the Ti_3C_2-TiO_2-AuNPs nano hybrid conjugated with numerous CD63 aptamer1 (Apt1) via Au-S band was captured on the exosomes, and the assembled electrode was detected the exosomes in the luminol pretreated by ultrasound. Scheme 1C shows the illustration for the synergistic effect of ultrasound-pretreatment and Ti_3C_2-TiO_2-AuNPs for the air-saturated luminol. The ultrasound-pretreatment strategy could generate superoxide radical ($O_2^{\bullet}$) and H_2O_2 effectively. More importantly, Ti_3C_2-TiO_2-AuNPs nanoprobes not only catalyze H_2O_2 but also aggregate ROS generated in situ via ultrasound-pretreatment, which can short the diffusion distance and improve the intermediate utilization rate, leading the enhancement of the ECL emission for the air-saturated luminol. The designed ECL biosensor can detect exosomes even in serum, blood, and urine samples, thus proving that it is a promising method for the routine monitoring of exosomes in clinical diagnostics.

2. Experimental

2.1. Materials and reagents

Reagents, materials, instruments, preparation of Ti_3C_2, Ti_3C_2-TiO_2 and Ti_3C_2-TiO_2-AuNPs are shown in Supplementary Material.

2.2. Exosome extraction and characterization

The culture of MDA-MB-231 cells and the extraction of exosomes refer to our previous work [5]. The TEM image of exosome revealed that the size of approximately is 50 nm [37] (Fig. S1).

2.3. Construction of the ECL platform

The glassy carbon electrode (GCE) with a diameter of 3 mm was polished with 0.3 and 0.05 μm alumina powder by turns and ultrasonic cleaning with ethanol and deionized water respectively. 6 μL of SA solution was modified on the GCE to form SA/GCE. Then, SA/GCE was activated in NHS and EDC (200 mM, 800 mM, v/v = 1:1) at 37°C for 1 h. Then, the SA/GCE was incubated in CD63 Apt2 (1 μM) at 37°C for 2 h to obtain Apt2/SA/GCE. Afterwards, different concentrations of exosomes (100 μL) were incubated on the Apt2/SA/GCE at 37°C for 2 h to form exosomes/Apt2/SA/GCE. The exosomes/Apt2/SA/GCE was incubated in 35 μL Ti_3C_2-TiO_2-AuNPs-Apt1 nanoprobes for 2 h to obtain an ECL biosensor. Finally, the ECL measurement was performed in luminol solution with ultrasound-pretreatment to detect exosomes. In each of the above steps, the electrode needs to be cleaned with ultrapure water and dried with N_2 to remove non-specific adsorption.

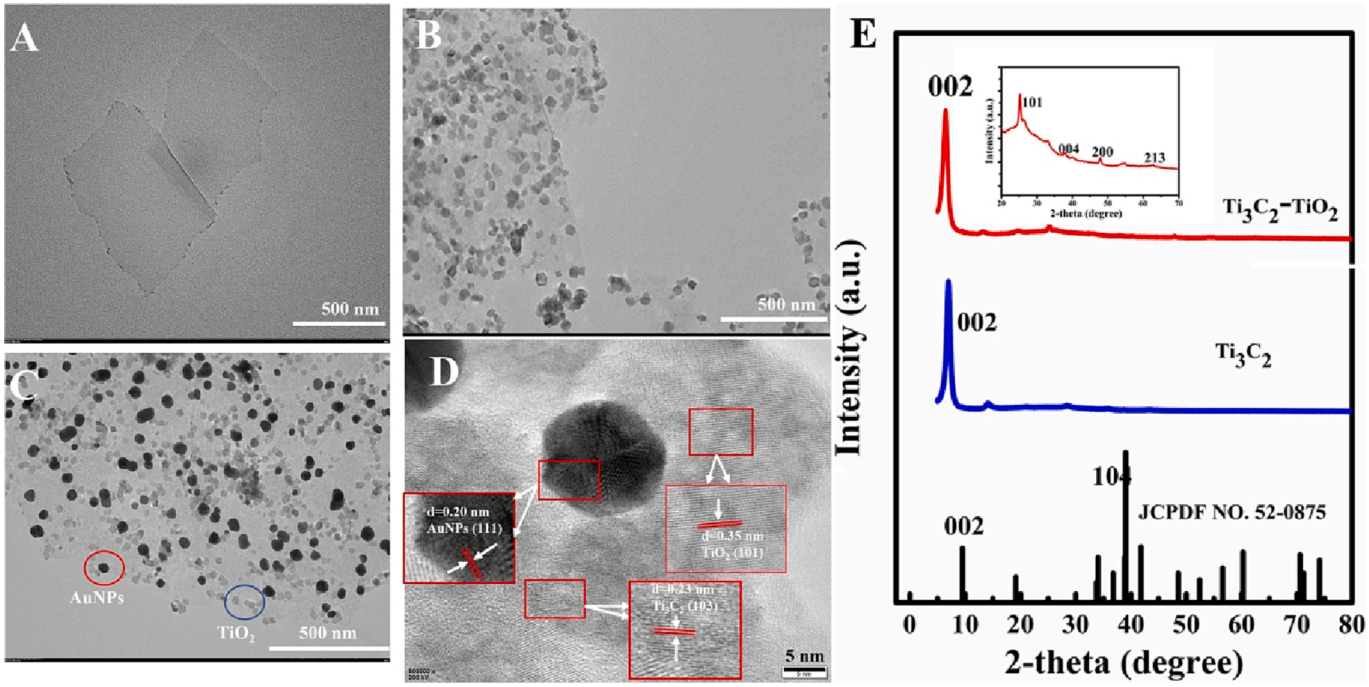

Fig. 1. The TEM images of Ti_3C_2 (A), Ti_3C_2-TiO_2 (B) and Ti_3C_2-TiO_2-AuNPs (C). The HRTEM image of Ti_3C_2-TiO_2-AuNPs (D). The XRD analyze of Ti_3C_2 and Ti_3C_2 -TiO_2 (E).

2.4. Ultrasound -pretreatment and ECL measurement

In this experiment, ultrasound was used as a pretreatment means. The air-saturated luminol solution (50 μM) was pretreated with ultrasound (7.5 W) at 1 MHz for 5 min, and then ultrasound was stopped and removed. Next, the modified electrode (Ti_3C_2-TiO_2-AuNPs-Apt1/exosomes/Apt2/SA/GCE) was used to detect exosomes in the pretreatment luminol solution.

In this work, a three-electrode system was used, the working electrode was the modified electrode, the reference electrode was Ag/AgCl (saturated KCl solution), and the auxiliary electrode was a platinum wire. The scanning potential was set from 0 to 0.6 V, and the scanning speed was 0.1 V s^{-1}. The PMT was 700 V.

3. Results and discussion

3.1. Characterization of the samples

To prove the preparation of Ti_3C_2-TiO_2 and Ti_3C_2-TiO_2-AuNPs, transmission electron microscopy (TEM), high resolution transmission

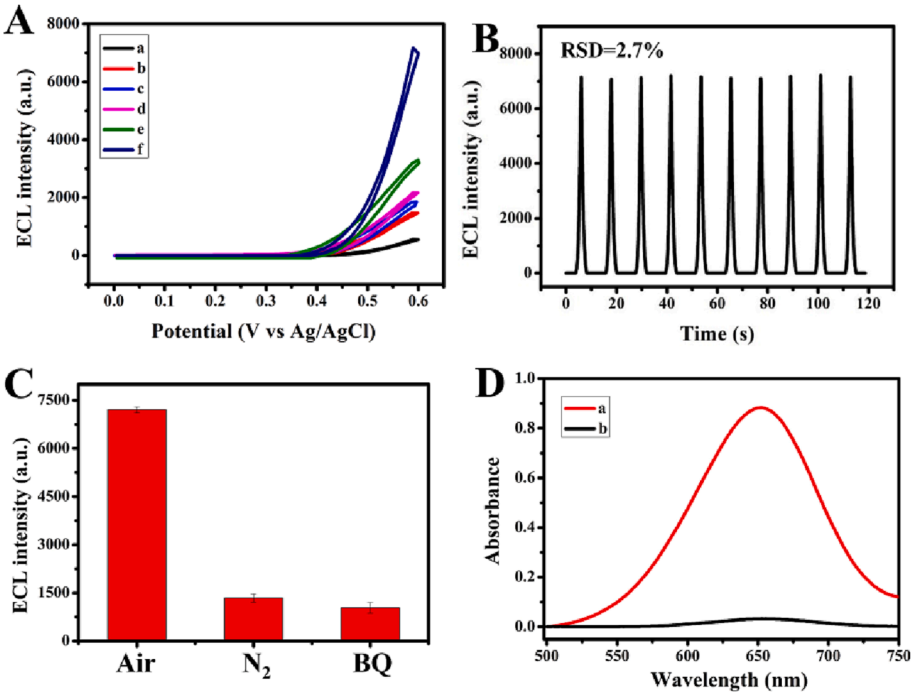

Fig. 2. (A) ECL-potential curves of (a) bare GCE, (b) Ti_3C_2/GCE, (c) Ti_3C_2-TiO_2/GCE, (d) Ti_3C_2-AuNPs/GCE and (e) Ti_3C_2-TiO_2-AuNPs/GCE in luminol. (f) Ti_3C_2-TiO_2-AuNPs/GCE in the air-saturated luminol with ultrasound-pretreatment. (B) The stability of Ti_3C_2-TiO_2-AuNPs/GCE in luminol with ultrasound-pretreatment. (C) ECL signal of the air-saturated luminol with ultrasound-pretreatment under different circumstances. (D) Absorption spectra of TMB* with ultrasound (a) and without ultrasound (b) pretreatment. Error bars are obtained by calculating the standard deviation of 3 parallel experiments.

electron microscope (HRTEM), X-ray diffraction (XRD) and X-ray photoelectron spectroscopy (XPS) characterization and EDS analysis were conducted. In the TEM image, the average diameter of Ti_3C_2 nanosheets was approximately 500 nm with smooth surfaces (Fig. 1A). After oxidation, the layered structure of Ti_3C_2 was retained and TiO_2 particles formed on the Ti_3C_2 nanosheets in situ can be observed (Fig. 1B and Fig. S2). The Ti_3C_2-TiO_2 was also characterized by XRD (Fig. 1E). The strongest peak of (1 0 4) crystal plane disappeared, the peak of (0 0 2) moved slightly to the left because of expansion of the interlayer of Ti_3C_2, which indicated that Ti_3C_2 nanosheets have been successfully synthesized. Meanwhile, the specific diffraction peaks of (1 0 1), (0 0 4), (2 0 0) and (2 1 3) crystal planes of TiO_2 appeared and the (0 0 2) peak of Ti_3C_2 existed, indicating that the Ti_3C_2-TiO_2 was successfully synthesized.

Moreover, the XPS full spectrum of Ti_3C_2-TiO_2 was shown in Fig. S3A. In the C1s spectra of Ti_3C_2-TiO_2 (Fig. S3B), the peak value (284.7 eV) belonged to adventitious carbon (C-C). The C1s spectra at 281.75 and 285.9 eV correspond to C-Ti and C-O. The wide peak at 455–465 eV, which were related with low valence and high valence Ti species. The peaks at ~455.4 eV and ~461.5 eV belonged to Ti-C and Ti-O bonds (Fig. S3C). The formation of Ti_3C_2-TiO_2 nano hybrid could lead to the transition of Ti (II) to Ti (IV). Two typical peaks of O1s of Ti_3C_2-TiO_2 appeared, which were related with Ti-O and C-Ti-Ox (Fig. S3D). The results showed that TiO_2 could be in-situ grown on Ti_3C_2.

The TEM and SEM images of the Ti_3C_2-TiO_2-AuNPs were shown in Fig. 1C and Fig. S4A, indicating that the AuNPs were dispersed on the Ti_3C_2 nanosheets. Furthermore, Fig. 1D was the HRTEM image of Ti_3C_2-TiO_2-AuNPs, it clearly exhibited the lattice fringe spacings of 0.23 and 0.35 nm, belonged to the (1 0 3) plane of Ti_3C_2 and the (1 0 1) plane of anatase TiO_2. Meanwhile, a clear lattice fringe spacing of about 0.20 nm could be observed, which was consistent with the Au (1 1 1) plane. The characterization of Ti_3C_2-TiO_2-AuNPs by EDS analysis was also proved. Ti and O elements came from Ti_3C_2 and TiO_2, C element came from the Ti_3C_2. Au element came from the AuNPs (Fig. S4B). In addition, in the UV–vis spectra (Fig. S4C), comparing with curve a, the absorption peak of Ti_3C_2-TiO_2 displayed red shift slightly (curve b). In the curve c, due to the surface plasma absorption of AuNPs, a characteristic absorption peak appeared at 550 nm approximately. The formation of Ti_3C_2-TiO_2-AuNPs was also recorded by the digital photo (Fig. S4D). The Ti_3C_2-TiO_2 was well dispersed in water with dark green (a), the $HAuCl_4$ solution resulted in yellow (b). In contrast, the mixture of Ti_3C_2-TiO_2 and $HAuCl_4$ leaded to purplish red (c), indicating reduction of $AuCl_4^-$ to form the Ti_3C_2-TiO_2-AuNPs. The EDS mapping of Ti_3C_2-TiO_2-AuNPs was shown in Fig. S5. C, O, Ti, F and Au elements appeared clearly, which could be more directly to demonstrate the successful synthesis of Ti_3C_2-TiO_2-AuNPs.

3.2. The effect of ultrasound-pretreatment and the Ti_3C_2-TiO_2-AuNPs

Firstly, the critical role of Ti_3C_2-TiO_2-AuNPs modified electrode in the air-saturated luminol with ultrasound-pretreatment for 5 min was studied. An ultralow ECL strength was gained on the bare GCE (Fig. 2A, curve a). After modification with Ti_3C_2, Ti_3C_2-TiO_2 and Ti_3C_2-AuNPs, Ti_3C_2-TiO_2-AuNPs, the ECL intensity was increased in turn (curve b, c, d and e). These results indicated that the Ti_3C_2-TiO_2-AuNPs nano hybrid showed the best electrocatalytic activity and conductivity than that of Ti_3C_2, Ti_3C_2-TiO_2 or Ti_3C_2-AuNPs. Amazingly, aiding by the ultrasound-pretreatment, the Ti_3C_2-TiO_2-AuNPs/GCE in the air-saturated luminol showed the highest ECL signal (curve f), which indicated that the ROS was generated in situ via the unique cavitation effect of ultrasound, which may be an important factor in enhancing ECL emission. In addition, the stability of the Ti_3C_2-TiO_2-AuNPs/GCE with ultrasound-pretreatment was studied under consecutive scanning for 10 cycles. These responses almost remained unchanged, and the RSD was 2.70% (Fig. 2B).

In addition to the ECL performance, the ECL enhancement mechanism was studied. As shown in the Fig. 2C, the Ti_3C_2-TiO_2-AuNPs/GCE exhibited a strong ECL emission in the air-saturated luminol with ultrasound-pretreatment, a low ECL strength was gained in the luminol which was saturated N_2 with ultrasound-pretreatment. These results showed that the dissolved oxygen was important in this system. It is well known that the $O_2^{\bullet-}$ was important as the intermediate, and it could oxidize luminol to 3-aminophthalate to generate ECL signal. Therefore, a commercially specific radical scavenger benzoquinone (BQ) for $O_2^{\bullet-}$ was introduced to confirm the nature of the involved reactive species. It was seen from the Fig. 2C, the addition of BQ induced 86 % quenching of the ECL signal, which confirmed that $O_2^{\bullet-}$ is mainly in the ROS generated by ultrasound-pretreatment and Ti_3C_2-TiO_2-AuNPs.

Since the reactive $O_2^{\bullet-}$ could yield H_2O_2 in the aqueous solution, we tended to confirm the existence of H_2O_2. The in-situ generation of H_2O_2 via ultrasound-pretreatment was validated by the H_2O_2 specific colorimetric method, in which HRP only catalyzed H_2O_2 to oxidize the substrate TMB to a colored product (TMB*, 650 nm). Compared with curve b in Fig. 2D, a specific absorbance was observed at about 650 nm by ultrasound-pretreatment (curve a), which confirmed the existence of H_2O_2. Moreover, the maximum absorption peak at 650 nm exhibited a linear fit with the H_2O_2 concentration (R^2 = 0.997) in the range of 10–50 μM (Fig. S6). According to the linear equation of A = -0.018 + 0.034C, the concentration of H_2O_2 generated by ultrasound-pretreatment was calculated as 26.47 μM.

The high-intensity focused ultrasound with the cavitation effect could form $O_2^{\bullet-}$ and H_2O_2 in situ as an initiator. Ti_3C_2-TiO_2-AuNPs was proved as a highly efficient booster, which could catalyze H_2O_2 to the $O_2^{\bullet-}$. The synergistic effects of ultrasound-pretreatment and Ti_3C_2-TiO_2-AuNPs greatly improved the ECL intensity in the air-saturated luminol. The ECL mechanism for the application of ultrasound-pretreatment and Ti_3C_2-TiO_2-AuNPs in the air-saturated luminol was proposed in Scheme 1C and Eqs. (1) - (6). A large amount of luminol anions (LH^-) were electrochemically oxidized to luminol anionic radicals ($L^{\bullet}$) [Eq. (1)]. Dissolved O_2 could obtain e^- on the electrode to produce $O_2^{\bullet-}$ [Eq. (2)]. Ultrasound-pretreatment effectively generated H_2O_2 and $O_2^{\bullet-}$ via cavitation effect [Eq. (3)]. Ti_3C_2-TiO_2-AuNPs could absorb and catalyze the H_2O_2 to generate more $O_2^{\bullet-}$ [Eq. (4)]. Lastly, excited-state intermediate (AP*) was formed via the reaction of $L^{\bullet-}$ with $O_2^{\bullet-}$, which returned to the ground state to obtain excellent ECL emission [Eq. (5) and (6)].

$$LH^- - e^- \rightarrow L^{\cdot-} + H^+ \quad (1)$$

$$O_2 + e^- \rightarrow O_2^{\cdot-} \quad (2)$$

$$O_2 \xrightarrow{Ultrasound} O_2^{\cdot-} + H_2O_2 \quad (3)$$

$$H_2O_2 \xrightarrow[catalyze\ and\ absorb]{Ti_3C_2-TiO_2-AuNPs} more\ O_2^{\cdot-} + H^+ \quad (4)$$

$$L^{\cdot-} + O_2^{\cdot-} \rightarrow AP^* + N_2 \quad (5)$$

$$AP^* \rightarrow AP + hv \quad (6)$$

3.3. Electrochemical characterizations of the ECL platform

Cyclic voltammetry (CV) was used to characterize the construction of this sensor. After modifying SA on bare electrodes, a smaller current (Fig. 3A, b) than that of the bare GCE (Fig. 3A, a) was shown distinctly. After Apt2 (c) and exosomes (curve d) were incubated, the peak current gradually decreased, because the non-conductive material retarded the electron transfer between the GCE and electroactive material. Finally, when the nanoprobes were connected to the surface of exosomes, the current significantly decreased, owing to the electron transport on electrode surface was blocked by the negatively charged nanoprobes (curve e). The assembly process of this biosensor was also characterized via electrochemical impedance spectroscopy (Fig. 3B). The SA, Apt2,

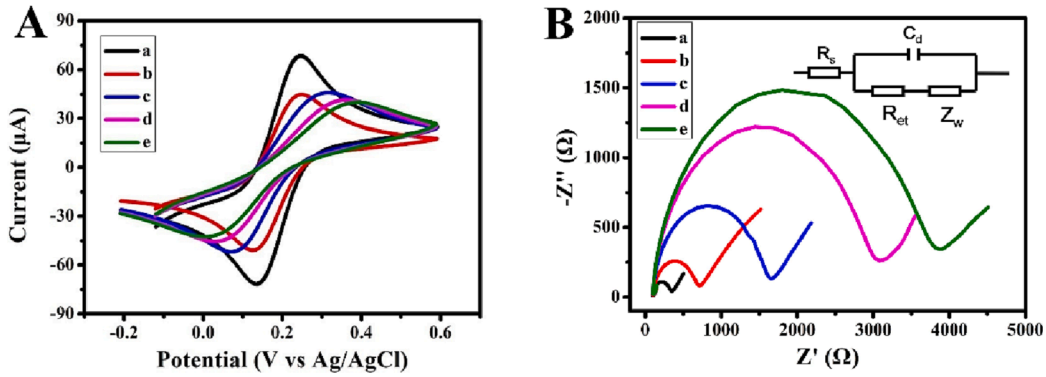

Fig. 3. (A) CV and (B) EIS curves of (a) bare GCE, (b) SA/GCE, (c) Apt2/SA/GCE, (d) exosomes/Apt2/SA/GCE and (e) Ti_3C_2-TiO_2-AuNPs-Apt1/exosomes/Apt2/SA/GCE in $[Fe(CN)_6]^{3-/4-}$.

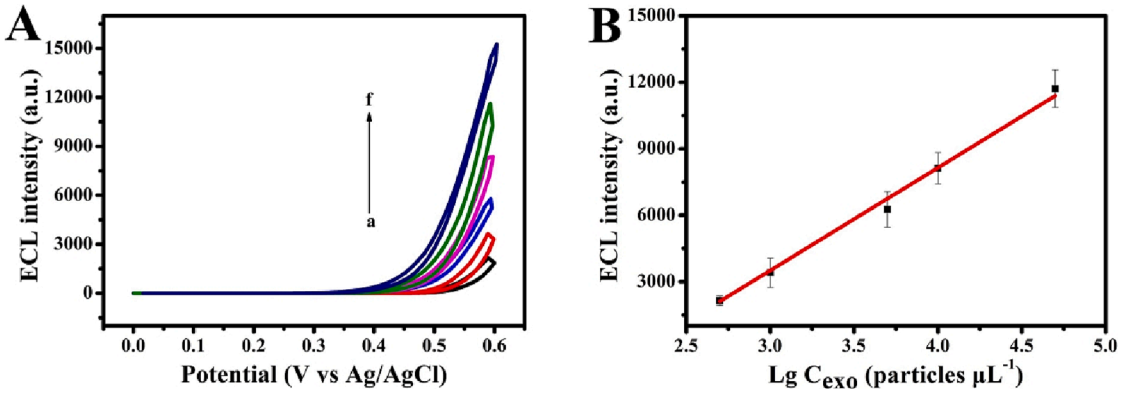

Fig. 4. (A) ECL response of this platform with different concentrations of exosomes (a-f: 5.0×10^2, 1.0×10^3, 5.0×10^3, 1.0×10^4, 5×10^4, 1.0×10^5 particles μL^{-1}, respectively) in the air-saturated luminol with ultrasound-pretreatment. (B) The corresponding linear calibration curve.

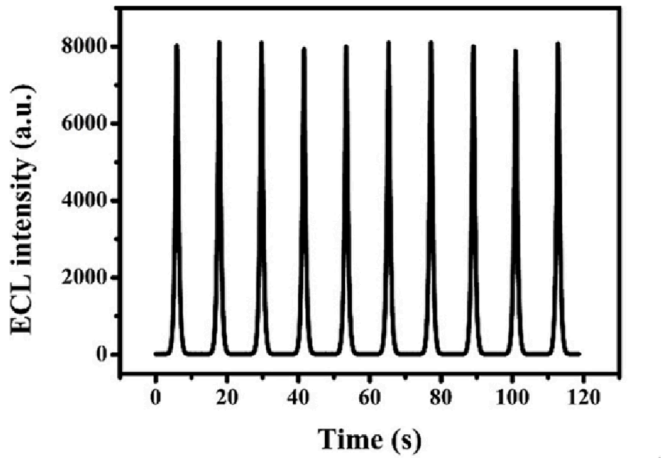

Fig. 5. Stability of the ECL sensor in luminol solution with ultrasound-pretreatment for 10 scans. The concentration of exosomes is 1.0×10^4 particles μL^{-1}.

exosomes and Ti_3C_2-TiO_2-AuNPs-Apt1 were modified on the GCE in turn, the arch became bigger gradually, indicating that charge-transfer resistance increased gradually. The above results indicated that the electrode assembly was successful.

3.4. Detection of exosomes

Exosomes are vesicles derived from cells (30–200 nm), which carry rich nucleic acids, proteins and lipids for intercellular communication. Because exosomes are highly related to the changes in physiological and pathological conditions for the diseases, especially cancer [38], they are widely considered as potential biomarkers for biological analysis and disease treatment.

The ECL intensity towards different concentrations of exosomes was studied under the optimal experimental conditions (Fig. S7). The ECL response increased with the concentration of exosomes increased from 5.0×10^2 to 1.0×10^5 particles μL^{-1} with a good linear relationship (Fig. 4A). The linear equation is I = -10411.56 + 4839.51LgC. The limit of detection (LOD) was 195 particles μL^{-1}, which was calculated via formula of LOD=(3σ-b)/k (σ is the background standard deviation, b is the intercept of the linear regression equation, and k is the slope of the linear regression equation), and the squared correlation coefficient (R^2) was 0.996. These results showed that this ECL platform had excellent performance for the exosome detection.

3.5. Stability and reproducibility of this platform

Moreover, measuring the ECL responses for 10 cycles was used to prove the stability, the ECL signals did not change significantly (Fig. 5). The reproducibility was evaluated via five Ti_3C_2-TiO_2-AuNPs-Apt1/exosomes/Apt2/SA/GCE, which was prepared by the same modification method. The RSD was 1.50% with 1.0×10^4 particles μL^{-1} exosomes for the ECL response of five electrodes, showing that this platform had excellent reproducibility.

3.6. Sample testing

The feasibility of the constructed sensors to detect target in actual

samples is important of clinical diagnosis. Exosomes (1.0×10^3 and 5.0×10^3 particles μL^{-1}) were added into serum, urine and blood samples for recovery experiments, respectively. The recovery rates are between 96.22% and 108.33% with the RSD of 1.67% to 5.51% (Table S1), showing that this biosensor had excellent anti-interference ability in complex matrix and showed potential in clinical sample detection.

4. Conclusion

A novel ECL sensor for detecting exosomes was designed through combining ultrasound-pretreatment with Ti_3C_2-TiO_2-AuNPs nano hybrid. Ultrasound-pretreatment as green and effective means could generate H_2O_2 and $O_2^{-\bullet}$ in situ via ultrasonic cavitation effect. Moreover, Ti_3C_2-TiO_2-AuNPs nano hybrid with strong catalytic performance could catalyze and aggregate ROS to generate more $O_2^{-\bullet}$, thereby enhancing ECL emission of the air-saturated luminol. As a proof of concept, the designed ECL platform was successfully used for exosome detection without additional co-reaction reagent. The LOD was 195 particles μL^{-1}. More importantly, this sensor could be used in detecting exosomes in serum, urine and blood. This green and concise method provides possibilities for the application of the air-saturated luminol.

5. Author statement

The authors declare that they have no known competing financial interests or personal relationships that could have appeared to influence the work reported in this paper. Neither the entire article nor any part of its content has been published or has been accepted elsewhere and is not submitted to any other journals.

Declaration of Competing Interest

The authors declare that they have no known competing financial interests or personal relationships that could have appeared to influence the work reported in this paper.

Data availability

No data was used for the research described in the article.

Acknowledgments

This work was financially supported by the Natural Science Foundation of Shandong Province (ZR2020MB063) and the Taishan Scholar Program of Shandong Province (ts201511027), China.

Appendix A. Supplementary data

Supplementary data to this article can be found online at https://doi.org/10.1016/j.ultsonch.2023.106330.

References

[1] C. Ma, Y. Cao, X. Gou, J.-J. Zhu, Recent progress in electrochemiluminescence sensing and imaging, Anal. Chem. 92 (1) (2020) 431–454.
[2] S. Liu, H. Yuan, H. Bai, P. Zhang, F. Lv, L. Liu, Z. Dai, J. Bao, S. Wang, Electrochemiluminescence for electric-driven antibacterial therapeutics, J. Am. Chem. Soc. 140 (6) (2018) 2284–2291.
[3] T. Zhuang, H. Zhang, L. Wang, L. Yu, Z. Wang, Anchoring luminol based on Ti_3C_2-mediated in situ formationof AuNPs for construction of an efficient probe for miRNA electrogenerated chemiluminescence detection, Anal. Bioanal. Chem. 413 (28) (2021) 6963–6971.
[4] S. Xu, X. Li, C. Li, J. Li, X. Zhang, P. Wu, X. Hou, In situ generation and consumption of H_2O_2 by bienzyme-quantum dots bioconjugates for improved chemiluminescence resonance energy transfer, Anal. Chem. 88 (12) (2016) 6418–6424.
[5] H. Zhang, Z. Wang, F. Wang, Y. Zhang, H. Wang, Y. Liu, In situ formation of gold nanoparticles decorated Ti_3C_2 MXenes nanoprobe for highly sensitive electrogenerated chemiluminescence detection of exosomes and their surface proteins, Anal. Chem. 92 (7) (2020) 5546–5553.
[6] L. Du, H.X. Zhang, Z.Y. Wang, T.T. Zhuang, Z.H. Wang, Boosting the electrochemiluminescence of luminol by high-intensity focused ultrasound pretreatment combined with 1T/2H MoS_2 catalysis to construct a sensitive sensing platform, Ultrason. Sonochem. 92 (2023), 106264.
[7] X.D. Zhu, H. Liu, Y.X. Dai, X.Y. Wang, C.N. Luo, Q. Wei, Enhanced electrochemiluminescence of luminol based on Cu_2O-Au heterostructure enabled multiple-amplification strategy, Biosens. Bioelectron. 151 (2020), 111970.
[8] X.M. Huang, X. Deng, W.J. Qi, D. Wu, Highly sensitive luminol electrochemiluminescence immunosensor based on platinum-gold alloy hybrid functionalized zinc oxide nanocomposites for catalytic amplification, Sensor. Actuat. B-Chem. 3273 (2018) 466–472.
[9] F.-F. Wu, Y. Zhou, H. Zhang, R. Yuan, Y.-Q. Chai, Electrochemiluminescence peptide-based biosensor with hetero-nanostructures as coreaction accelerator for the ultrasensitive determination of tryptase, Anal. Chem. 90 (3) (2018) 2263–2270.
[10] W. Gu, H. Wang, L. Jiao, Y.u. Wu, Y. Chen, L. Hu, J. Gong, D. Du, C. Zhu, Single-atom iron boosts electrochemiluminescence, Angew. Chem. Int. Ed. 59 (9) (2020) 3534–3538.
[11] F.A. Bushira, P. Wang, Y. Wang, S. Hou, X. Diao, H. Li, L. Zheng, Y. Jin, Plasmon-boosted Fe, Co dual single-atom catalysts for ultrasensitive luminol-dissolved O_2 electrochemiluminescence detection of prostate-specific antigen, Anal. Chem. 94 (27) (2022) 9758–9765.
[12] F.A. Bushira, S.A. Kitte, C. Xu, H. Li, L. Zheng, P. Wang, Y. Jin, Two-dimensional-plasmon-boosted iron single-atom electrochemiluminescence for the ultrasensitive detection of dopamine, hemin, and mercury, Anal. Chem. 93 (28) (2021) 9949–9957.
[13] W. Gu, X. Wang, J. Wen, S. Cao, L. Jiao, Y.u. Wu, X. Wei, L. Zheng, L. Hu, L. Zhang, C. Zhu, Modulating oxygen reduction behaviors on nickel single-atom catalysts to probe the electrochemiluminescence mechanism at the atomic level, Anal. Chem. 93 (24) (2021) 8663–8670.
[14] Y.Y. Pu, H.H. Yin, C.H. Dong, H.J. Xiang, W.C. Wu, B.G. Zhou, D. Du, Y. Chen, H. X. Xu, Sono-controllable and ROS-sensitive CRISPR-Cas9 genome editing for augmented/synergistic ultrasound tumor nanotherapy, Adv. Mater. 33 (2021) 2104641.
[15] A. Zhou, T. Fang, K. Chen, Y. Xu, Z. Chen, X. Ning, Biomimetic activator of sonodynamic ferroptosis amplifies inherent peroxidation for improving the treatment of breast cancer, Small 18 (12) (2022) 2106568.
[16] X.P. Li, L.Z. Zheng, Advances of high intensity focused ultrasound (HIFU) for pancreatic cancer, Int. J Hyperthermia. 29 (2013) 678–682.
[17] Y. Zheng, D. She, H. Huang, L. Lin, S. Chen, Y. Lu, L.i. Liu, Z. Pang, B.o. Yin, Versatile nanocompositeaugments high-intensity focused ultrasound for high-efficacy sonodynamic therapy of glioma, Nano Res. 15 (10) (2022) 9082–9091.
[18] Q. Li, J. Zhang, J. Li, H. Ye, M. Li, W. Hou, H. Li, Z. Wang, Glutathione-activated NO-/ROS-generation nanoparticles to modulate the tumor hypoxic microenvironment for enhancing the effect of HIFU-combined chemotherapy, ACS Appl. Mater. Interfaces 13 (23) (2021) 26808–26823.
[19] X. Pan, H. Wang, S. Wang, X. Sun, L. Wang, W. Wang, H. Shen, H. Liu, Sonodynamic therapy (SDT): a novel strategy for cancer nanotheranostics, Sci China Life Sci. 61 (4) (2018) 415–426.
[20] H. Zhang, L. Du, Z. Wei, X. Wang, N. Sojic, X. Zhou, Z. Wang, Boosting the electrochemiluminescence of luminol-O_2 system by high intensity focused ultrasound, Anal. Bioanal. Chem. 414 (29-30) (2022) 8309–8315.
[21] F. Takahashi, R. Shimizu, T. Nakazawa, J.Y. Jin, Potential-modulated electrochemiluminescence of a tris(2,2′-bipyridine)ruthenium(II)/lidocaine system under 430 kHz ultrasound irradiation, Ultrason. Sonochem. 63 (2020), 104947.
[22] C.Y. Tian, L. Wang, F. Luan, X.M. Zhuan, An electrochemiluminescence sensor for the detection of prostate protein antigen based on the graphene quantum dots infilled TiO_2 nanotube arrays, Talanta 191 (2019) 103–108.
[23] Y.T. Huang, S.P. Zhang, L. Lv, Z.S. Hong, H. Dai, Y. Lin, Integrated heterojunction and photothermal effect multiple enhanced ratiometric electrochemiluminescence immunosensor based on calcination controlled and tunable TiO_2 mesocrystals, Sensor. Actuat. B-Chem. 346 (2021), 130565.
[24] T.-T. Tu, Y. Sun, Y.-M. Lei, Y.-Q. Chai, Y. Zhuo, R. Yuan, Pyrenecarboxaldehyde encapsulated porous TiO_2 nanoreactors for monitoring cellular GSH levels, Nanoscale 14 (15) (2022) 5751–5757.
[25] X.M. Huang, X. Deng, K. Sua, W.J. Qi, Enhanced electrochemiluminescence of Au-Ag bimetallic nanocluster@CNTs-TiO_2 nanocomposite and its use in ultra-sensitive immunosensing for CEA, New J. Chem. 45 (2021) 13064.
[26] X.G. Ma, C. Wang, F.X. Wu, Y.R. Guan, G.B. Xu, TiO_2 Nanomaterials in Photoelectrochemical and Electrochemiluminescent Biosensing, Topics Curr. Chem. 37 (2020) 28.
[27] X. Wei, C. Xiao, C. Liu, K.e. Wang, Y. Tu, The sensitized solid-phase electrochemiluminescence of electrodeposited poly-luminol/aniline on AuAg/TiO_2 nanohybrid functionalized electrode for flow injection analysis, Electroanalysis 26 (4) (2014) 807–814.
[28] Y.Z. Wang, H. Zhong, X.R. Li, G.Q. Liu, K. Yang, M. Ma, L.L. Zhang, J.Z. Yin, Z. P. Cheng, J.K. Wang, Nonenzymatic electrochemiluminescence glucose sensor based on quenching effect on luminol using attapulgite-TiO_2, Sensor. Actuat. B-Chem. 230 (2016) 449–455.
[29] X.P. Wu, X. Zhong, Y.Q. Chai, R. Yuan, Electrochemiluminescence acetylcholine biosensor based on biofunctional AMs-AChE-ChO biocomposite and electrodeposited graphene-Au-chitosan nanocomposite, Electrochim. Acta 147 (2014) 735–742.
[30] Z.W. Seh, K.D. Fredrickson, B. Anasori, J. Kibsgaard, A.L. Strickler, M. R. Lukatskaya, Y. Gogotsi, T.F. Jaramillo, A. Vojvodic, Two-dimensional

molybdenum carbide (MXene) as an efficient electrocatalyst for hydrogen evolution, ACS Energy. Lett. 1 (3) (2016) 589–594.
[31] H.X. Zhang, T.T. Zhuang, L. Wang, L. Du, J.F. Xia, Z.H. Wang, Efficient Au nanocluster@Ti_3C_2 heterostructure luminophore combined with Cas12a for electrochemiluminescence detection of miRNA, Sensor. Actuat. B-Chem. 370 (2022), 132438.
[32] M. Naguib, V.N. Mochalin, M.W. Barsoum, Y. Gogotsi, 25th anniversary article: MXenes: A aew family of two-dimensional materials, Adv. Mater. 26 (2014) 992–1005.
[33] H.X. Zhang, Z.H. Wang, F. Wang, Y.M. Zhang, H.Y. Wang, Y. Liu, Ti_3C_2 MXene mediated prussian blue in situ hybridization and electrochemical signal amplification for the detection of exosomes, Talanta 224 (2021), 121879.
[34] R. Tang, S. Xiong, D. Gong, Y. Deng, Y. Wang, L. Su, C. Ding, L. Yang, C. Liao, Ti_3C_2 2D MXene: Recent progress and perspectives in photocatalysis, ACS Appl. Mater. Interfaces 12 (51) (2020) 56663–56680.
[35] L. Wang, H.X. Zhang, T.T. Zhuang, J.X. Liu, N. Sojic, Z.H. Wang, Sensitive electrochemiluminescence biosensing of polynucleotide kinase using the versatility of two-dimensional $Ti_3C_2T_X$ MXene nanomaterials, Anal. Chim. Acta 1191 (2022), 339346.
[36] Z. Wei, H. Zhang, Z. Wang, High-intensity focused ultrasound combined with Ti_3C_2-TiO_2 to enhance electrochemiluminescence of luminol for the sensitive detection of polynucleotide kinase, ACS Appl. Mater. Interfaces 15 (3) (2023) 3804–3811.
[37] A. Cynthia, M. Sepideh, K. Houman, A. Milad, S.S.Z. Mohammad, J. Mahsa, S. Dariush, B. Behzad, D. Masood, K. Tohid, Docosahexaenoic acid (DHA) inhibits pro-angiogenic effects of breast cancer cells via down-regulating cellular and exosomal expression of angiogenic genes and microRNAs, Life Sci. 258 (2020), 118094.
[38] S. Wan, L. Zhang, S. Wang, Y. Liu, C. Wu, C. Cui, H. Sun, M. Shi, Y. Jiang, L. Li, L. Qiu, W. Tan, Molecular recognition-based DNA nanoassemblies on the surfaces of nanosized exosomes, J. Am. Chem. Soc. 139 (15) (2017) 5289–5292.